City Research Online

City, University of London Institutional Repository

This is the accepted version of the paper.

This version of the publication may differ from the final published version.

High speed laser surface modification of Ti–6Al–4V

Evans Chikarakara ⬚, Sumsun Naher, Dermot Brabazon
Dublin City University, Glasnevin, Dublin 9, Ireland

Abstract

Titanium and its alloys have been commonly used for biomedical implant applications for many years; however, associated high coefficient of friction, wear characteristics and low hardness have limited their long term performance. This article investigates the effects of the high speed laser surface modification of Ti–6Al–4V on the microstructure, surface roughness, meltpool depth, phase transformation, residual strain, microhardness, and chemical composition. Laser treatment was carried out using a 1.5 kW CO_2 laser in an argon gas environment. Irradiance and residence time were varied between 15.7 to 26.7 kW/mm2 and 1.08 to 2.16 ms respectively. Laser treatment resulted in a 20 to 50 μm thick surface modified layer without cracks. An increase in residence time and irradiance resulted in higher depth of processing. Surface roughness was found to decrease with increase in both irradiance and residence time. Metallography showed that a martensite structure formed on the laser treated region producing acicular α-Ti nested within the aged β matrix. The laser treatment reduced volume percentage of β-Ti as compared to the non-treated surface. Lattice stains in the range of 0.81% to 0.91% were observed after laser surface modification. A significant increase in microhardness was recorded for all laser treated samples. Microhardness increased up to 760 HV0.05 which represented a 67% increase compared to the bulk material. Energy Dispersive X-ray Spectroscopy (EDS) analysis showed that laser surface modification produced a more homogenous chemical composition of the alloying elements compared to the untreated bulk metal.

1. Introduction

Ti–6Al–4V is the most frequently and successfully used titanium alloy in biomedical engineering due to its favourable properties: high strength to weight ratio, low density and biocompatibility. Despite the aforementioned qualities, Ti–6Al–4V has poor surface properties which lead to wear and corrosion when used in harsh environments like the human body. Studies showed that patients with titanium alloy implants had at least threefold increase in Ti ion concentration in their serum compared to patients without implants [1–3]. Release and accumulation of metallic ions overtime by the way of passive dissolution or another process involving wear can potentially lead to discoloration of the surrounding tissue or an inflammatory reaction causing pain and even leading to loosening owing to osteolysis [4–6]. For titanium alloys to be used in transmission components, such as hip implants, where there are severe friction conditions, the problems of surface wear via adhesive and abrasive mechanisms, and subsurface damage via plastic deformation from contact loading need to be overcome [7–9].

Since these properties of titanium alloys depend on the surface layer, rather than the bulk alloy, surface modification could provide a solution to allow implant longevity enhancement. Laser surface modification of titanium and its alloys is known to improve mechanical and tribological properties. Laser surface modification plays a dual role: minimizing the release of metal ions by making the surface of the alloy harder and, more corrosive and wear resistant; as well as making the surface more bioactive and stimulating bone growth due to improvement in wettability and lower local surface energies [8,10]. To increase tribological properties of the alloy surface, most operations generally relied on forming a hard nitrogen rich surface layer by ion or laser techniques [11–14]. Laser alloying techniques such as nitriding are known to produce uncontrollable cracks, poor result reproducibility and non-homogeneous weak layers due to the complexity in dissolving the material uniformly in the melted pool [15]. Advantages presented by laser surface melting compared to other surface modification techniques include: superior bonding, reduced distortion, improved physical properties (hardness and wear), and easier control over depth of processing [16,17]. Ti– 6Al–4V was of interest in this study due to its workability and the ability to produce refined microstructures which are otherwise unachievable in other titanium alloys [18,19]. This paper presents laser surface melting under an argon environment to prevent oxidation and alloying with air elements during processing. The work utilised high speed laser processing capable of combinations of lower irradiances and higher residence times compared to previous research [20–25]. Low residence time allows for higher cooling rates, thus producing a more dynamic solidification which allows for novel phase formation and more homogeneous microstructures. The novel focus of this work was to apply combinations of high irradiance and low residence times to gain an understanding of the resultant microstructure, surface roughness, meltpool depth, phase transformation, residual strain, microhardness and chemical composition mechanisms.

2. Experimental

The experiments were conducted on conventional biomedical titanium alloy Ti–6Al–4V. Composition of the as-received annealed alloy is listed in Table 1. The workpiece, 100 mm long, 20 mm wide and 4 mm high, was grit blasted prior to laser treatment in order to remove surface defects from the alloy. Grit blasting is also known to improve the absorption of the laser wavelength by creating a nonreflective surface [26]. This was carried out using inert soda lime glass with particles ranging between 106 and 212 μm. The samples were ultrasonic cleaned for 10 min at 60 °C, before and after laser treatment to remove tightly adhering particles embedded onto the surfaces during grit blasting. A 1.5 kW CO_2 laser was used in continuous mode to irradiate the workpiece at three levels of irradiance: 15.72, 20.43 and 26.72 kW/ mm2 and three levels of residence time: 1.08, 1.44 and 2.16 ms, see Table 2. The Gaussian laser beam was focused on the work-piece surface providing a laser spot size of 90 μm. A schematic of the laser processing set-up is shown in Fig. 1. The residence time is the period for which the laser beam was in contact with a unit area of the workpiece [27]. Irradiation was carried out using a raster

scan with a partial overlap of 30% in order to provide for microstructural and compositional homogeneity. Argon at a pressure of 200 kPa was used as an assist gas to avoid oxidation during laser processing. The laser beam was kept perpendicular to the workpiece during laser irradiation to maximise the absorbance and ensure uniform conditions for processing. The influence of the process parameters on the microstructure of the modified surface topology and cross section was studied by using optical and scanning electron microscopy (SEM) with the aim of providing a better understanding of the process. For cross sectional examination after grinding and polishing, etching was carried out by immersion in Kroll's reagent for 60–90 s. Composition of the etchant was distilled water H_2O (92 ml), nitric acid HNO_3 (6 ml) and Hydrofluoric acid HF (2 ml). This etching procedure allowed optical examination of the microstructural features including grain size, phase features and meltpool depth. Ten measurements were taken using the SEM to obtain the average meltpool depth for each sample. Surface mean roughness (Ra) measurements were performed using a stylus profilometer. Sampling and evaluation lengths used were 0.8 mm and 4 mm respectively. Five measurements were taken to obtain the average roughness for each sample, according to ISO 4287/4288. Vickers microhardness test was performed using a set load of 500 mN and 30 s indentation time. X-ray diffraction patterns of the samples were recorded using a Bruker D8 XRD system, with Cu-Kα (λ=1.5405 Å) radiation. The diffraction patterns were recorded in the 2θ range of 20 to 90°. Strain and residual stress calculation induced by laser treatment were calculated by using the variation in the value of interplanar spacing (d) calculated from shifting of the diffraction peaks [28]. Energy Dispersive Spectroscopy (EDS) was used to determine the chemical composition of the treated layer. Confidence intervals displayed for all results were calculated using the t-distribution at 95% confidence.

Table 1
As received Ti–6Al–4V element composition (wt.%).

Element	C	Si	Fe	O	V	Al	Ti
wt.%	0.14	0.01	0.16	0.17	3.97	6.36	Balance

Table 2
Laser processing parameters used in the experimental design.

Sample ID	Power (W)	Irradiance (kW/mm^2)	Sample speed (mm/min)	Residence time (ms)
1	100	15.72	2500	2.16
2	130	20.44		
3	170	26.72		
4	100	15.72	3750	1.44
5	130	20.44		
6	170	26.72		
7	100	15.72	5000	1.08
8	130	20.44		
9	170	26.72		

3. Results

3.1. Morphology and microstructure characterisation Fig. 2 presents the topographic and cross-sectional views of the asreceived Ti–6Al–4V. There were no observable voids, inclusions, pits or cracks present. Fig. 3 presents the topographical characteristics of the laser treated region, highlighting the regular processing tracks at a constant residence time of 1.08 ms and at the three levels of irradiance 15.72, 20.4 and 26.7 kW/mm2. The BSE images show no evidence of ablation of the surface. The width of the tracks is representative of the laser beam spotsize of 90 μm. Effects of irradiance on surface roughness can also be inferred from Figs. 3 and 4 which reveal the cross sectional microstructure of the laser treated Ti–6Al–4V corresponding to Fig. 3. The sample treated at higher irradiance showed a smoother surface finish compared to the samples treated at lower irradiance. High speed laser treatment resulted in the creation of a crack-free modified layer ranging from 20 to 50 μm thick with very different microstructures compared to the bulk alloy. The laser treated region lacked a discernible grain structure and heat affected zone, which are prevalent in other laser treatment processes in literature [20]. Excellent bonding was observed in the modified layers processed in this work which is typical of laser surface processing.

3.2. Roughness characterisation

The measured average roughness of the grit blasted alloy was 0.56±0.1 μm. The laser surface processing subsequently produced average roughness values between 1.39 μm and 2.73 μm. Fig. 3 illustrates the effect of irradiance on roughness at a residence time of 1.08 ms. Fig. 5 graphs the effect of irradiance and residence time on roughness. Roughness was found to decrease with increase of irradiance and residence time. A combination of low residence time and low

irradiance produced the highest roughness due to a more unevenly melted surface produced by the lower energy density, where energy density is the product of irradiance and residence time.
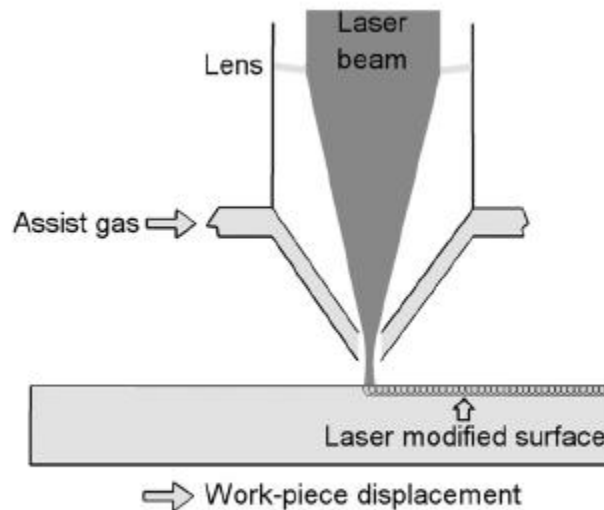

Fig. 1. Schematic of the laser processing set-up.

3.3. Meltpool depth characterisation

Fig. 4 highlights the changes in roughness, grain structure and meltpool depth of the laser modified regions. Increase in both irradiance and residence times resulted in an increase in meltpool depth as shown in Fig. 6. Micrographs in Fig. 4 show that irradiance has an effect on the thickness uniformity of the melted area. As the irradiance increased, a more homogeneous meltpool depth with fewer discontinuities was observed. Lower meltpool depths were obtained in this experiment compared to other laser surface modification studies [20,21].

3.4. X-ray diffraction characterisation

Backscatter images of the laser treated surfaces provided an ideal starting point for further phase microanalysis by highlighting presence of two phases. The as-received Ti–6Al–4V consisted of a mixture of α and β-Ti. The relative volume fraction of β-Ti was lower than that of α-Ti. The α and β phases present in untreated Ti–6Al–4V alloy are clearly visible in the backscattered electron detector microstructure image shown in Fig. 7(a). Subsequent to laser processing, the α-Ti phase was transformed into an acicular structure. The microstructure of the treated Ti–6Al–4V revealed that the transformed acicular α-Ti was nested within the aged β matrix, see Fig. 7(b). The corresponding X-ray diffraction patterns presented in Fig. 7(c) and (d) further confirmed the presence of these phases. The shift in diffraction peaks to a new 2θ position within the laser treated samples, in Fig. 7(d), depicts a uniform microstrain within the structure [27]. Table 3 lists the phase volume distribution and lattice strain of untreated and laser treated Ti–6Al–4V. A reduction in volume fraction of β-Ti up to 12% following melting was observed.
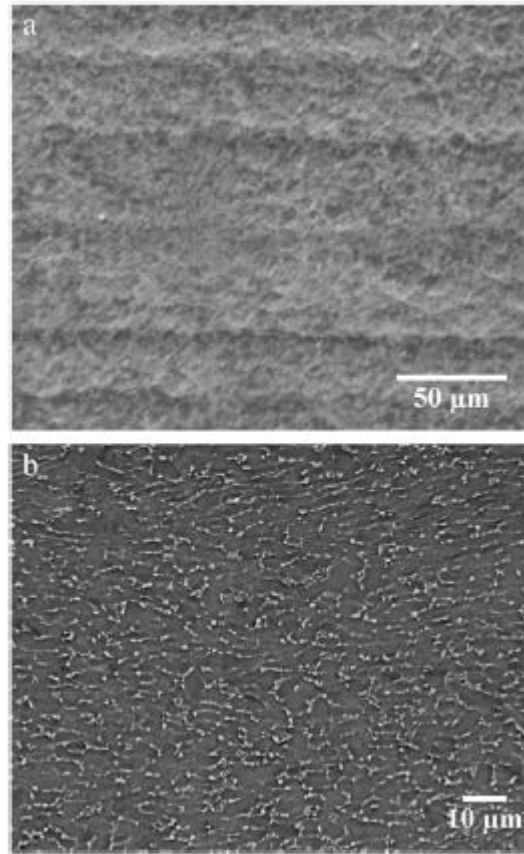
Fig. 2. SEM images of the as-received Ti–6Al–4V (a) topography and (b) cross-section.
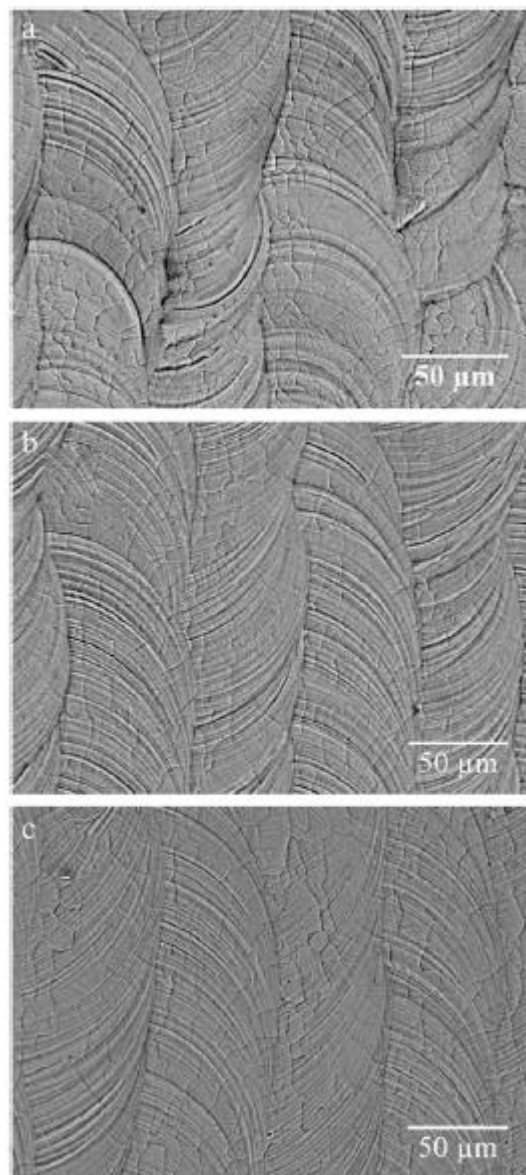
Fig. 3. Back scatter detector (BSE) surface morphology images of laser surface modified Ti–6Al–4V at a constant residence time of 1.08 ms and three levels of irradiance (a) 15.72, (b) 20.4 and (c) 26.7 kW/mm².
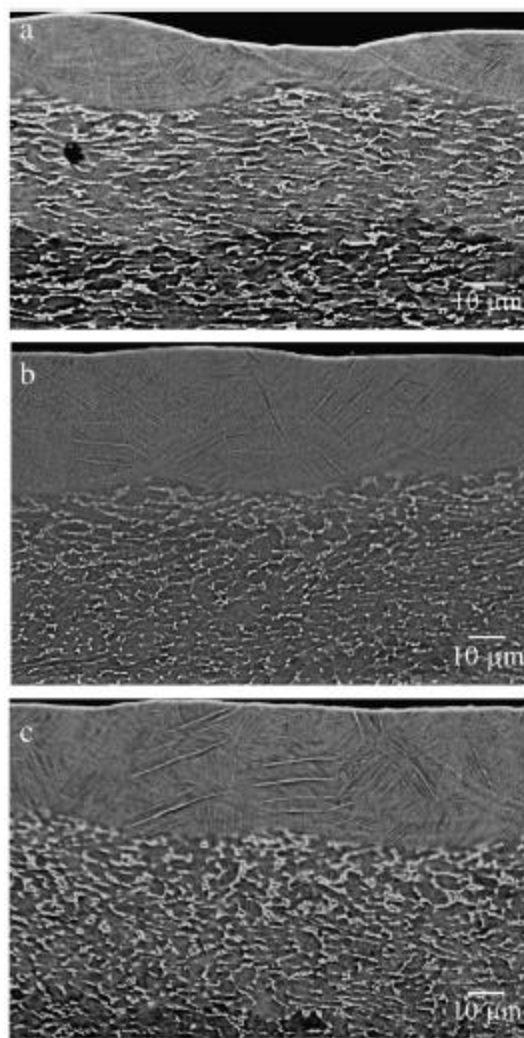
Fig. 4. Cross-sectional BSE images of laser treated Ti–6Al–4V corresponding to processed surfaces shown in Fig. 2 (a), (b) and (c).

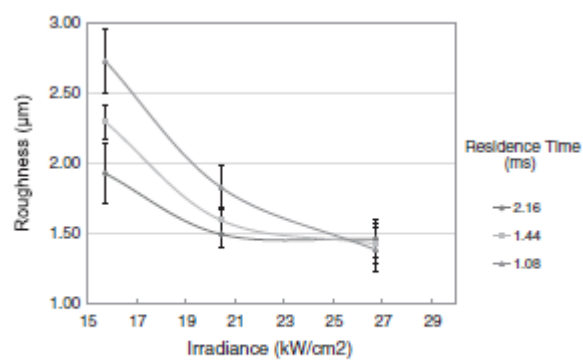

Fig. 5. Effects of irradiance and residence time on average roughness of the Ti–6Al–4V samples.
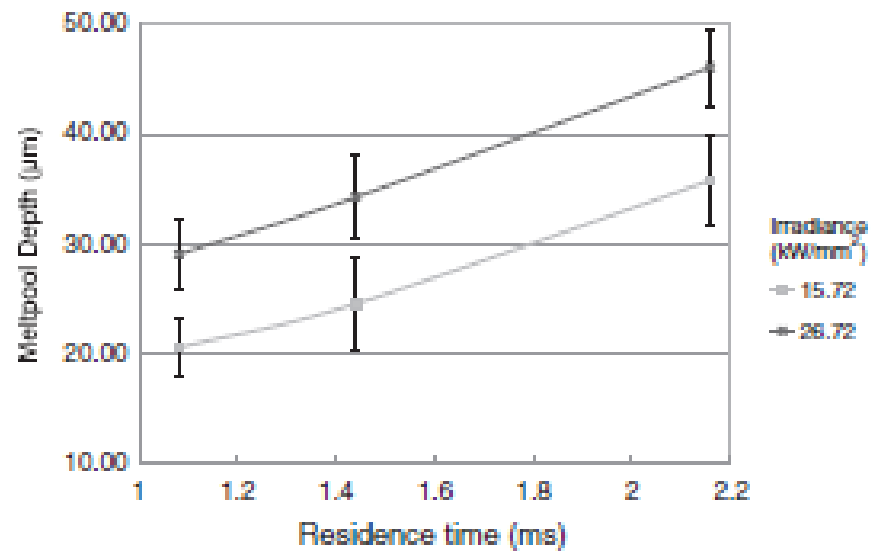
3.6. Energy-dispersive X-ray spectroscopy (EDS)

Fig. 9(a) shows the microstructure of the laser treated Ti−6Al−4V, each line spectrum representing a point of analysis 8 μm apart. EDS results from samples 3, 6 and 9 (see Table 2) are shown in Fig. 9(b). Fig. 9(b) reveals the titanium composition corresponding to the spectrum points shown in Fig. 9(a). Within the laser treated region, the titanium element composition was uniform at 90% compared to the relatively non-homogenous titanium distribution within the bulk alloy. The same trend was found for the vanadium and aluminium alloying elements.

4. Discussion

4.1. Morphology and microstructure Processing parameters used in this study were carefully chosen so that energy densities do not exceed levels that induce ablation of surface material. Lack of ejected material or channel-like features in the BSE images can be evidenced as absence of ablation of the surface. Instead, the surface was melted and rapidly solidified due to high speed processing. Unlike other surface modification techniques that have three distinct regions: modified region, heat affected zone and the bulk alloy; this type of laser treatment does not show a discernible heat affected zone [20]. Formation of this structure was due to the rapid solidification which thwarted the segregation of the various alloying elements into high and low concentration. The exclusion of cracks and the lack of a heat affected zone, from the experimental conditions examined in this work, indicate a surface modification technique that can be successfully applied and is well adjacent to the bulk metal. Crack elimination is attributed to the high speed processing, low residence times and corresponding assist gas parameters. These processing characteristics ensure minimal thermal stress was exerted on the surface thus avoiding crack development.

4.2. Roughness

The decrease in roughness is mainly attributed to a more homogenous melting produced at high irradiance thus producing smoother surfaces. The process used in this study is laser surface melting and it highly depends on the residence time and irradiance. The product of the two which is energy density can be used to limit the process to just melting. At certain energy densities the material gets ablated producing cutting effects. Preliminary experimental design studies found that a further increase in irradiance at high residence times would cause ablation an associated rise in roughness. Roughness variation thus depends on energy density. In this experiment an energy density of approximately 29 J/mm2 (samples 9) produced preeminent homogeneity with the lowest roughness.

Fig. 6. Effects of laser irradiance and residence time on meltpool depth for the Ti–6Al–4V samples.
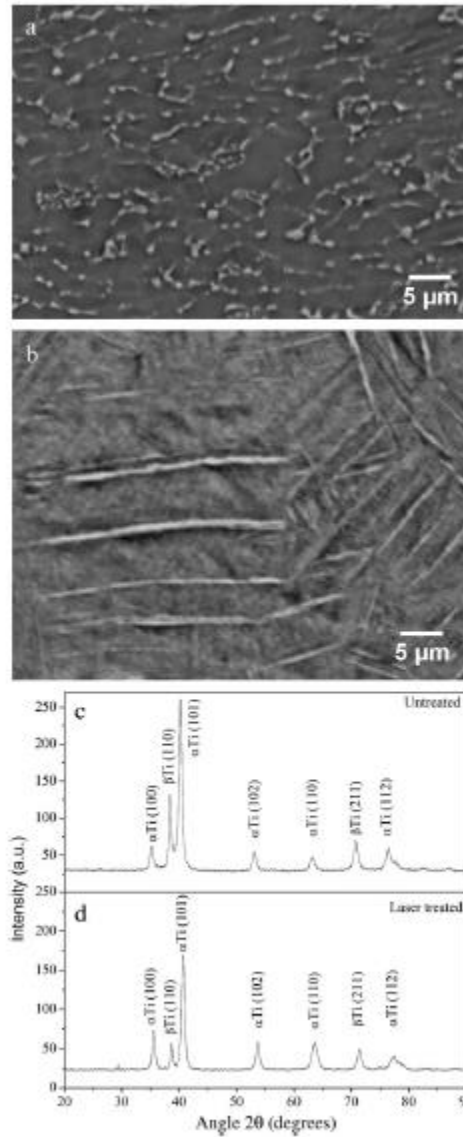
Fig. 7. BSE microstructural images of (a) untreated and (b) laser treated Ti–6Al–4V, and X-ray diffraction pattern of (c) untreated and (d) laser treated Ti–6Al–4V.

Table 3

Phase distribution and lattice strain of as received, grit blasted and laser treated Ti–6Al–4V.

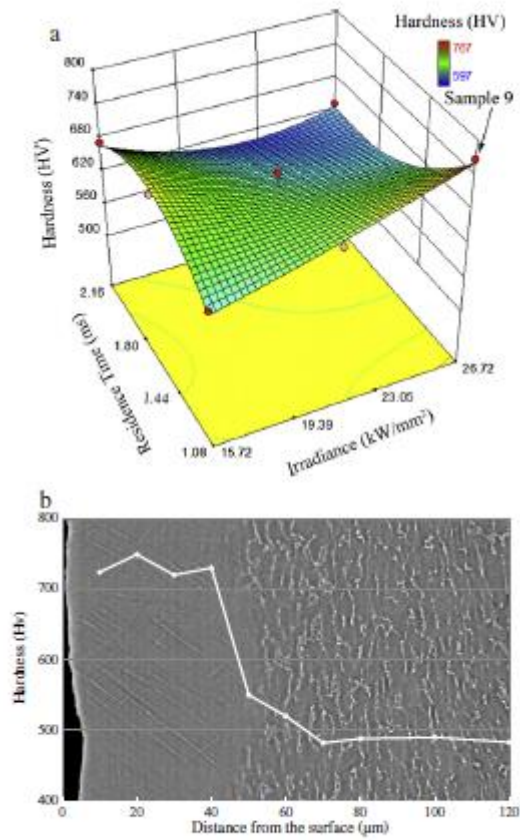| Sample	Processing parameters	Volume phase	Lattice strain (%)
As-received	N/A	72% αTi	N/A
		28% βTi	
Laser modified	Residence time — 1.08 ms	84% αTi	0.91
	Irradiance — 15.72 kW/mm^2	16% βTi	0.81

Fig. 8. (a) Micro hardness distribution for all samples taken at the midpoint of the treated surface and (b) the microhardness with respect to depth from the surface for sample 9.

4.3. Meltpool depth

Meltpool depth is crucial in contact components since the depth of the modified layer is related to the lifetime of the component. The meltpool profile not only depends on energy density but also on the laser beam profile used which was TEM00 (Gaussian). This beam profile becomes more perceptible in the microstructure at low irradiance and residence times, as seen in Fig. 4. Fig. 4 also highlights that there is no significant change in depth of processing between samples irradiated at 20.4 and 26.72 kW/mm2; this is due to insignificant difference in energy densities, 22 and 29 J/mm2 respectively. However, the significance can be easily demonstrated for samples treated at irradiances of 15.72 and 26.72 kW/mm2 as seen in Fig. 6; this is due to a higher difference in energy density. Meltpool depths are lower than other laser processing treatments found in literature due to the low residence time, induced by high sample speeds and a low beam spotsize used in this work. Lower meltpool depths can be advantageous due to their corresponding lower induced thermal stress thus eliminating formation of cracks on the surface.

4.4. X-ray diffraction analysis

The phase structure transformation from the typical α+β structure into a fine martensite structure was due to the low residence times used in the experiments which resulted in high cooling rates. Such high cooling rates force formation of different composition phases but allow very little time for diffusion to produce those phases' equilibrium compositions [9]. Acicular martensite

structure enhances the materials wear and corrosion resistance. A decrease in β phase in the microstructure is known to improve corrosion properties since pitting attacks mainly target the β phase [29]. The reduction of volume fraction of β-Ti following melting is attributed to the stabilisation of acicular martensite in the structure during rapid quenching [22]. Laser treatment of Ti–6Al–4V induced uniform strain generated over relatively large distances, thus changing the lattice plane spacings in the constituent grains from a stress free value to a new value corresponding to the magnitude of stress applied. Broadening of diffraction peaks is known to represent non-uniform microstrain. Since no broadening effects occurred, it can be concluded that only uniform microstrain was caused by the laser processing parameters. Microstrain is induced within the melted zone of the surface treated Ti– 6Al–4V samples mainly due to a very high thermal gradient developed and the related quench stress built thereafter. 4.5. Microhardness analysis The increase of hardness produced as a result of the laser treatment is caused by the refinement of microstructure and the formation of acicular martensite during rapid quenching. This fine, acicular martensite has a hexagonal closed packed structure and possesses a high hardness but relatively low ductility and toughness [9,30]. Uniformly high hardness levels throughout the laser modified region iterate the superiority of the modified regions compared to the bulk alloy. High hardness and uniformity of the modified layer is important in biomedical Ti–6Al–4V alloys as it has a significant influence on wear resistance properties [31,32]. 4.6. Energy-dispersive X-ray spectroscopy (EDS) Uniform element distribution in the modified region could be due to high speed of convection stream providing intensive stirring of the elements inside the molten pool as well as the high cooling rates prohibiting sufficient time for elemental diffusion and segregation typical under slower cooling conditions. Re-distribution of alloying elements within the treated titanium alloys is also known to improve pitting corrosion resistance due to preferential corrosion attack prevention [33].

5. Conclusions
High speed laser melting of Ti-6Al-4V in an inert argon environment produced a modified layer from 20 to 50 μm deep with improved microstructural properties. The microstructure of the laser modified layer was transformed to acicular α embedded within β matrix due to high cooling rates experienced. No cracks were observed in the laser treated layer. A relationship between irradiance and residence time for roughness was observed, whereby roughness decreased with an increase in irradiance and residence time. Roughness characteristics were closely related to the melting intensity and energy density. An increase in residence time and irradiance resulted in an increased depth of processing. Higher irradiance levels were found to provide for a more uniform depth of processing which reached a maximum of 50 μm. X-ray diffraction results demonstrated an increase of α phase in Ti–6Al–4V subsequent to laser treatment. Laser surface modification introduced residual strain 0.81% to 0.91% within the modified region. Microhardness examination revealed an increase of up to 67% subsequent to laser treatment. EDS analysis verified improved homogenous chemical composition of the modified layer due to redistribution of elements as a result of rapid solidification. The associated low residence time and rapid cooling rates allowed for novel and apparently useful properties to be achieved.
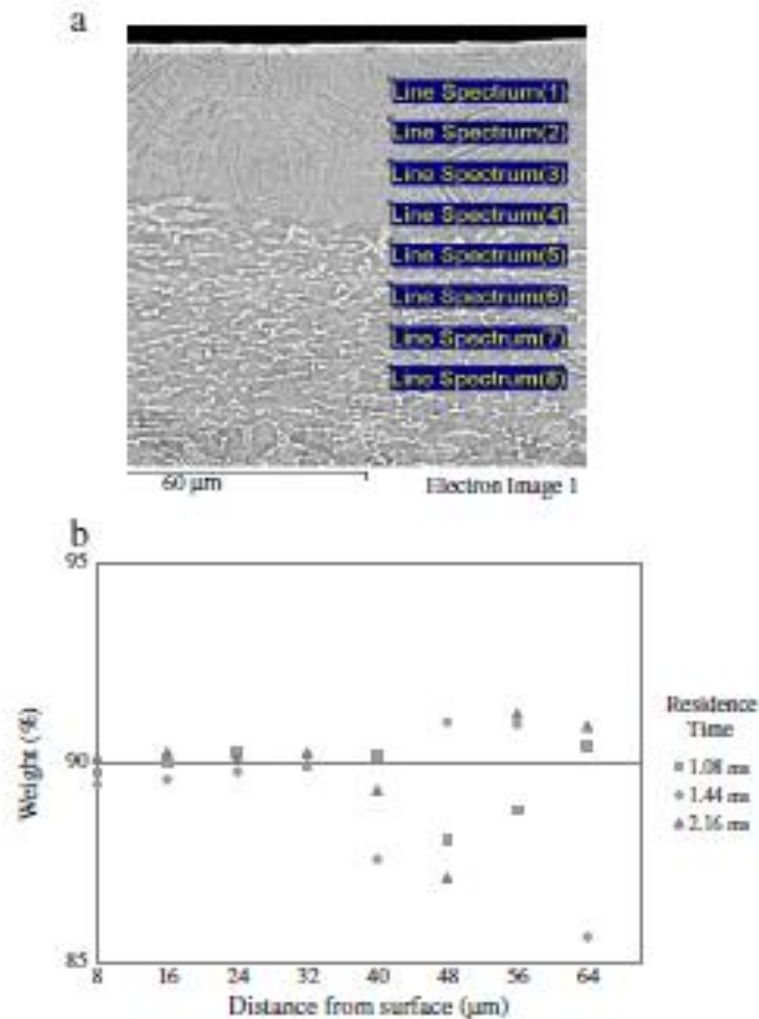
Fig. 9. (a) Cross-sectional BSE images of the laser treated Ti–6Al–4V highlighting the sampling distances (b) EDS of titanium composition distribution in samples 3, 6 and 9.

References

[1] J.J. Jacobs, A.K. Skipor, L.M. Patterson, N.J. Hallab, W.G. Paprosky, J. Black, J.O. Galante, J. Bone Joint Surg. Am. 80 (1998) 1447.
[2] S.S. Leopold, R.A. Berger, L. Patterson, A.K. Skipor, R.M. Urban, J.J. Jacobs, J. Arthroplasty 15 (2000) 938.
[3] J.J. Jacobs, C. Silverton, N.J. Hallab, A.K. Skipor, L. Patterson, J. Black, J.O. Galante, Clin. Orthop. 358 (1999) 173.
[4] J.T. Scales, J. Bone Joint Surg. Br. 73 (1991) 534.
[5] D. Granchi, E. Cenni, G. Trisolino, A. Giunti, N. Baldini, J. Biomed. Mater. Res. B 77B

(2006) 257.

[6] N.J. Hallab, K. Mikecz, C. Vermes, A. Skipor, J.J. Jacobs, J. Biomed. Mater. Res. 56 (2001) 427.

[7] A. Gaggl, G. Schultes, W.D. Muller, H. Karcher, Biomaterials 21 (2000) 1067.

[8] L. Hao, Laser Surface Treatment of Bio-Implant Materials, Wiley, West Sussex, 2005.

[9] R.R. Boyer, in: G. vander Voort (Ed.), ASM Handbook Volume 09: Metallography and Microstructures, ASM International, Ohio, 2004, p. 458.

[10] N. Mirhosseini, P.L. Crouse, M.J.J. Schmidth, L. Li, D. Garrod, Appl. Surf. Sci. 253 (2007) 7738.

[11] L. Xiuyan, Y. Jiaorong, T. Bin, Adv. Mater. Res. 79−82 (2009) 695.

[12] T.R. Jervis, T.G. Zocco, K.M. Hubbard, M. Nastasi, Metall. Mater. Trans. A 24 (1993) 215.

[13] H.C. Man, N.Q. Zhao, Z.D. Cui, Surf. Coat. Technol. 192 (2005) 341.

[14] B.S. Yilbas, M. Khaled, C. Karatas, I. Uslan, O. Keles, Y. Usta, M. Ahsan, Surf. Coat. Technol. 201 (2006) 679.

[15] Y.S. Tian, C.Z. Chen, D.Y. Wang, T.Q. Lei, Surf. Rev. Lett. 12 (2005) 123.

[16] W.M. Steen, K.G. Watkins, J. Phys. IV 3 (1993) 581.

[17] P. Jiang, X.L. He, X.X. Li, L.G. Yu, H.M. Wang, Surf. Coat. Technol. 130 (2000) 24.

[18] F.H. Froes, D. Eylon, C. Suryanarayana, J. Metall. 42 (1990) 26.

[19] J. Qazi, J. Rahim, F.S. Fores, O. Senkov, A. Genc, Metall. Mater. Trans. A 32 (2001) 2453.

[20] Z. Sun, I. Annergren, D. Pan, T.A. Mai, Mater. Sci. Eng. A-Struct. A345 (2003) 293.

[21] R. Singh, A. Kurella, N.B. Dahotre, J. Biomater. Appl. 21 (2006) 49.

[22] A. Biswas, L. Li, T.K. Maity, U.K. Chatterjee, B.L. Mordike, I. Manna, J. Dutta, Lasers Eng. 17 (2007) 59.

[23] T.M. Yue, J.K. Yu, Z. Mei, H.C. Man, Mater. Lett. 52 (2002) 206.

[24] C. Langlade, A.B. Vannes, J.M. Krafft, J.R. Martin, Surf. Coat. Technol. 100−101 (1998) 383.

[25] D. Brabazon, S. Naher, P. Biggs, Solid State Phenom. 141−143 (2008) 255.

[26] W.M. Steen, J. Mazumder, K. Watkins, Laser Material Processing, fourth ed. Springer, 2010.

[27] A.N. Samant, B. Du, S.R. Paital, S. Kumar, N.B. Dahotre, J. Mater. Process. Technol. 209 (2009) 5060.

[28] B.D. Cullity, S.H. Stock, Elements of X-ray Diffraction, third ed. Prentice Hall, New Jersey, 2001.

[29] M. Atapour, A. Pilchak, G.S. Frankel, J.C. Williams, M.H. Fathi, M. Shamanian, Corrosion 66 (2010) 1.

[30] K. Ferjutz, J.R. Davis, in: D.L. Olson, T.A. Siewert, S. Liu, G.R. Edwards (Eds.), ASM Handbook, ASM International, Ohio, 1990.

[31] N. Axén, S. Jacobson, S. Hogmark, Tribol. Int. 27 (1994) 233.

[32] T.N. Baker, in: H. Dong (Ed.), Surface Engineering of Light Alloys — Aluminium, Magnesium and Titanium Alloys, CRC Press, 2009.

[33] M. Geetha, U.K. Mudali, N.D. Pandey, R. Asokamani, B. Raj, Surf. Eng. 20 (2004) 68.